Molecular BioSystems

Accepted Manuscript

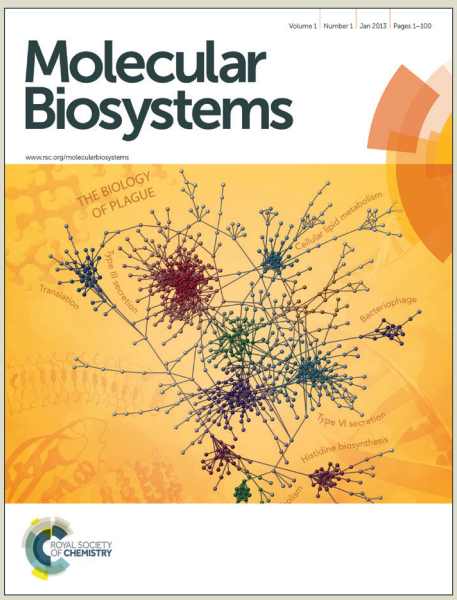

ROYAL SOCIETY OF CHEMISTRY

www.rsc.org/molecularbiosystems

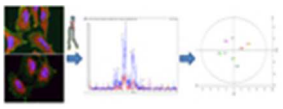

11x4mm (300 x 300 DPI)

A lipidomics investigation of the induced hypoxia stress on HeLa cells by using MS and NMR techniques

Yang Yu[a,b], Laura Vidalino[b], Andrea Anesi[a], Paolo Macchi[b] and Graziano Guella [*a,b,c]

Abstract

Induced hypoxia stress on cervical cancer derived cells (HeLa cells) leads to significant changes of their membrane lipid profiles. The lipidome of HeLa cells was characterized by a joint approach wherein liquid chromatography-mass spectrometry (LC-MS) analysis was followed by high resolution NMR measurements. Multivariate data analysis showed apparent separation between control and hypoxia-treated HeLa cells and thus demonstrated hypoxia effects on lipid metabolism. The most striking finding was that hypoxia stimulation significantly reduced the total amount of cellular phosphoinositols (PI) but caused a prominent increase of the amount of lyso phosphocholines (lyso-PC) and lyso phosphoethanolamines (lyso-PE). The observed attenuation of PI amount upon hypoxic conditions is probably due to the accumulation of cellular myo-inositol, which is known to play a critical role in d*e novo* synthesis of PI. Moreover, our study suggests that polyunsaturated phospholipids species are stronger biomarkers for discriminating the effect of hypoxia treatment. The evaluation of changes in the average unsaturation index (UI) of the membrane lipids acyl chains reveals that UI slightly increases in several lipid classes, thus affecting membrane fluidity and further membrane-dependent functions. The plausible mechanisms by HeLa cells to adapt to hypoxia conditions are also briefly reported.

Key words: HeLa/ hypoxia/ lipidomics/ NMR/ mass spectrometry/multivariate analysis

Introduction

[a] *Bioorganic Chemistry Laboratory, Department of Physics, University of Trento, Trento, Italy*
[b] *Molecular and Cellular Neurobiology lab, CIBIO Centre for Integrative Biology, University of Trento, Trento, Italy*
[c] *CNR, Istituto di Biofisica, Trento, Via alla Cascata 56/C, 38050 Povo (TN) – Italy*
**Email :graziano.guella@unitn.it*
Fax :+39 461281696
Tel :+39 461 281536

As an emerging field, lipidomics represents the global identification and quantitative assessment of the vast array of lipids, or lipidome, within a given biological system.[1,2] To achieve such a comprehensive description, lipidomics involves system-level analysis of thousands of pathways and networks of cellular lipid species as well as their interactions with other factors including other lipids or proteins.[3] Cellular membranes are composed of complicated arrangements of lipids which participate in vital cellular functions. Phospholipids (PL) and sphingolipids (SL), the major components of cellular membranes, exert important cellular functions associated with cell proliferation, apoptosis, signal transduction pathways and regulation of membrane trafficking.[4] The major PL classes present in mammalian cellular membranes are 1,2 diacyl-glycerophospholipids such as glycerophosphocholines (PC), glycerophosphoethanolamines (PE), glycerophosphoinositols (PI), glycerophosphoglycerols (PG), glycerophosphoserines (PS), glycerophosphatidic acids (PA) as well as the corresponding 1-alkenyl,2-acyl analogues such as plasmenyl-PC (pPC) and plasmenyl-PE (pPE). Among the sphingosine-based (SL) membrane lipids, N-acylated ceramides (Cer), sphingomyellins (SM which are 1-O phosphocholine ceramide derivatives) and galactosylceramides (Gal-Cer) are usually found as important membrane components in eukaryotic cells. The structural diversity of all these lipid classes, often leading to several hundreds of individual molecular species, is essentially caused by the acyl chains structural diversity which in turn derives from diversity in their chain length and degree of unsaturation. Other important cellular lipids are lyso-phospholipids (lyso-PL) bearing only one acyl chain at the sn-1 position (usually) of the glycerol backbone which are involved in important signaling pathways. Growing evidence has correlated the perturbation of lipid metabolism as well as dysfunctions of specific lipid species to a variety of diseases including cancer, obesity, hypertension, diabetes and neurodegenerative diseases.[5] Thus, lipidomics represents an important tool to study alterations in lipid metabolism and can facilitate the discovery of lipid biomarkers as useful indicators of disease progression or metabolic cellular response to various environmental stressors.

The greatest advances in lipidomics investigations have been relied on two main analytical techniques, the nuclear magnetic resonance (NMR) and the mass spectrometry (MS), the latter often coupled to a liquid chromatography (LC) system. As a non-destructive and highly reproducible technique,[6] NMR is often used in lipids analysis for *ab initio* structural elucidation of new lipid species; however, due to its intrinsically quantitative response, it can be, used even

for reliable quantifications of lipids mixtures obtained by tissues, body fluids and cell cultures.[4,7] In particular, ^{31}P-NMR spectroscopy is a very powerful technique in the quantitation of PL classes due to the fact that, at least in principle, within a given PL class the phosphorous nucleus feels a different chemical environment with respect to that of a different PL class. Owing to the high sensitivity and resolution for characterization of intact lipid species, electrospray ionization mass spectrometry coupled with liquid chromatography (LC-ESI MS) can supply the most comprehensive and informative data set for cellular lipidome studies.[8] Tandem MS measurements, for example, through precursor ion scanning and neutral loss scanning, are also often required for identification of all lipid molecular species. This latter methodology is usually much better than full scan MS due to its higher sensitivity and enhanced signal/noise ratio and, therefore, can facilitate the characterization of minor but biologically relevant lipid species.[9]

HeLa cellular lipidome has been rarely studied. As a model system, lipidomic analysis of HeLa cells has been performed to analyze the response of eight classes of phospholipids to paclitaxel-induced apoptosis by combing normal phase liquid chromatography (NPLC)/ESI (negative ionization)/MS^n-based lipidomic strategy with multivariate statistical analysis.[10] The aim of this study was to explore the relation between phospholipids metabolism and paclitaxel-induced apoptosis as well as phospholipase changes to better understand the anticancer mechanisms of chemotherapeutic agents. HeLa cellular lipidome study has been also conducted using the shotgun lipidomic approach to investigate cell cycle dependent changes in membrane stored curvature elastic energy by analyzing lipid composition alterations in different cell phases, revealing that HeLa cells can modify the membrane stored elastic energy through cell cycles.[11] These previous works have suggested HeLa cell line is a good model in lipidomic research with respect to anticancer drug effects on global lipid metabolism and to energy homeostasis related lipid profile alterations.

Increasing evidence shows that cancer cells are correlated with specific alterations in lipid metabolism. In fact, changes in lipid composition are strongly related to many cellular processes, including cellular growth, proliferation, energy homeostasis and motility.[12] Cells derived from prokaryotic and eukaryotic organisms have the abilities to sense and respond to oxygen alterations to maintain their homeostasis. In particular, cancer cells have developed oxygen-sensing capability to adapt to chronic low-oxygen conditions,[13] known as hypoxia. Previous studies have demonstrated that tumor hypoxia has been associated with changes in

carbohydrate and lipid metabolism. For cancer cells, low oxygen availability can lead to the activation of hypoxia-inducible factor (HIF), which causes the switch of cellular metabolic processes to anaerobic energy production including prevention of glucose-derived lipid synthesis and requirement of glutamine as carbon source for lipid synthesis.[12] Recently, few studies proposed phospholipids as reliable markers for hypoxia that induces alterations in tumor cell proliferation[14] and it is believed that lipidomics tool is promising for future and more comprehensive studies of cancer cellular lipid profile alterations induced by hypoxia. Nevertheless, more information and global phospholipids profile analysis as well as its interrelated cellular pathways still remain to be revealed.

In order to address the hypoxia-mediated alterations in cancer cellular phospholipid profile, to elucidate the corresponding pattern, and to further reveal the underlying mechanisms as well as molecular pathways involved, we performed a lipidomics investigation using HeLa cell line as a model system. First, we characterized each phospholipid class and individual phospholipid molecular species in control and hypoxia-stressed HeLa cells by resorting to the high resolution NMR and high performance liquid chromatography (HPLC) – ESI QqQ MS/MS tecniques. Second, multivariate data analysis (MVDA) was used to differentiate control and hypoxia-stressed cells and to understand how (existence of potential lipid biomarkers) and how much the changes in phospholipid profile are able to get light into the targeted biological problem (hypoxia). Finally, the trends and the possible mechanisms for such changes have been investigated by analyzing changes in the overall unsaturation index of PL classes. Taken together, our data show for the first time how the cell membranes lipids of HeLa cancer cells are affected by induced-hypoxia states and provide a preliminary insight into the corresponding mechanisms.

Materials and Methods

Chemicals

Methanol was of hypergrade for LC-MS with purity 99.9% (Merck). Chloroform with purity 99.8% and water were of HPLC grade (VWR). Ultrapure water was obtained from Milli-Q system (Millipore). Methanol-D4 was with deuteration degree of min. 99.8% for NMR Spectroscopy (Merck). Lipid standards DLPC (1,2-dilauroyl-*sn*-glycero-3-phosphocholine), DOPC (1,2-dioleoyl-*sn*-glycero-3-phosphocholine), DOPS (1,2-dioleoyl-*sn*-glycero-3-phospho-

L-serine), DOPA (1,2-dioleoyl-*sn*-glycero-3-phosphate), DSPG (1,2-dioctadecanoyl-sn-glycero-3-phospho-(1'-rac-glycerol)) and standards SM (sphingomyelin, Brain, Porcine), L-α-PE (Egg, Chicken), L-α-PI (Soy) with purity >99% were all purchased from Avanti Polar Lipids (Alabaster). Standard lipids and extracted cellular lipids were prepared and dissolved in glass vials.

Cell culture and Hypoxia treatment

HeLa cells were cultured in DMEM (supplemented with 10% heat-inactivated FBS, 1% L-glutamine and 1% penicillin/ streptomycin) in an incubator at 37 $^{\circ}$C with 5% CO_2. 24 hours before hypoxia treatment, HeLa cells were synchronized by serum starvation. Hypoxia was induced with 200 μM Cobalt (II) chloride ($CoCl_2$) added to cell cultures for 3h. Untreated cells were used as negative controls. In order to achieve sufficient biomass for NMR analysis, approximately $1x10^8$ cells were used, while $1x\ 10^7$ cells were sufficient for MS analysis. Since cell cultures are growing in strictly controlled conditions, their variability is smaller than the one expected for other type of samples, thus allowing the use of smaller sample sizes (n=4).

Immunocytochemistry and fluorescence microscopy

Cell cultures were carried out as described previously (Vidalino *et al.,* 2012). After $CoCl_2$ treatment, HeLa cells were washed in pre-warmed PBS and then fixed in 4% PFA for 15 minutes at room temperature. After permeabilization in 0.1% Triton X100 for 5 minutes, cells were immunostained. The following antibodies were used: mouse anti-HIF1α (dilution 1:50; Abcam), rabbit anti-ACTIN (dilution 1:500, Sabta Cruz. The following secondary antibodies (1:500, Invitrogen) were used: Alexa Fluor 488-conjugated goat anti-rabbit and anti-mouse IgGs, Alexa Fluor 594-conjugated. Microscopy analysis was performed using the Zeiss Observer Z.1 Microscope implemented with the Zeiss ApoTome device and with a PlanApo oil immersion lens (63X, NA=1.4). Pictures were acquired using AxioVision imaging software package (Zeiss) and assembled with Adobe Photoshop 7.0. Images were not modified other than adjustments of levels, brightness and magnification.

Phospholipids extraction and sample preparation

Total cellular lipids were extracted according to Bligh and Dyer method with slight modifications.[15] In brief, medium was removed and cells washed with PBS twice followed by trypsin digestion. Cells were washed again with PBS and centrifuged for 10 min at r.t. at 2400 g. The pellet was then resuspended in 1 ml Milli-Q water and incubated in ice. Before lipid extraction, 10 ng/µl standard DLPC (12:0/12:0), distinct from any natural cellular lipid as previously assessed, was added in order to estimate the yield of extraction (recovery). 3 ml chloroform/methanol (v/v 2:1) was added to the resuspended pellet followed by sonication in ice (program set as total time 15 min, amplitude 20, time pulse 3 sec and time pause 5 sec). The samples were then centrifuged at 16000 g for 10 min at 4 °C and the chloroform phase (bottom layer) was carefully collected into a glass vial and the upper layer was subjected to another extraction step. The combined chloroform fractions were evaporated under a gentle stream of N_2. The extracted lipids were initially dissolved in 700 µl of perdeuterated methanol (CD_3OD) for NMR measurements. At the end of NMR analysis the sample was then concentrated to final volume of 500 µl and used for all the MS analysis. The final standard DLPC (12:0/12:0) concentration assuming a 100% recovery was 6.25 ng/µl. Peak area of DLPC in the real sample was divided by that of DLPC in standard solution (6.25 ng/ul assuming 100% recovery) to give the value of lipid recovery.

NMR measurements

^{1}H- (400 MHz) and ^{31}P-NMR (162 MHz) spectra of the raw organic lipid extracts were recorded in d_4-methanol (99.90% CD_3OD) at 300 K on a Bruker-Avance 400 MHz NMR spectrometer by using a 5 mm BBI probe equipped with pulsed-gradient field utility. The ^{1}H-90^0 proton pulse length was found 9.3 µs with a transmission power of 0 db whilst ^{31}P-90^0 proton pulse length was 17 µs with a transmission power of -3 db. The chemical shift scale (δ) was calibrated on the residual proton signal of CD_3OD at δ_H 3.310 ppm and δ_C 49.00 ppm whilst the ^{31}P-NMR δ scale was calibrated on the PC signal at δ_P -0.550 ppm. The following experiments were done (info obtained are reported in brackets): ^{1}H-NMR (proton chemical shifts and scalar couplings J); ^{1}H-^{1}H DQCOSY (proton-proton scalar correlation); ^{1}H–^{13}C HSQC (proton-carbon one-bond correlation); ^{1}H–^{13}C HMBC (proton-carbon multiple-bond correlation). 1D NMR spectra (^{1}H and ^{31}P) of the lipid extracts were fitted and integrated by the software MestreNova 8.1 (Mestrelab Research S.L., Escondido, CA).

Optimization of precursor ion scanning and neutral loss scanning for ESI MS/MS analysis

Characteristic fragmentation of each standard phospholipid (PL) class (DOPC, DOPS, DOPA, DSPG, SM, L-α-PE (Egg), L-α-PI (Soy)) were firstly studied by triple quadruple mass spectrometry (Applied Biosystems API 3000^{TM}, Italy) with direct infusion at 10 µl /min using a syringe pump (Harvard Apparatus, Italy). Individual standard lipid was dissolved in methanol/water (v/v 7:3) containing ammonium acetate (10 mM). Full scan and MS/MS analysis were performed both in positive and negative ionization mode. Next, equal volume of 1 mg/ml of each lipid standard were mixed and analyzed by HPLC - ESI MS/MS to optimize class-specific MS/MS head group survey scanning (Precursor Ion Scanning and Neutral Loss Scanning) for sample analysis.

HPLC-ESI MS/MS measurements

Total HeLa PL extracts were separated and analyzed with Shimadzu High Performance LC^{TM} (CBM-20 A, equipped with the binary pump LC-20AB, Italy) combined with Applied Biosystems API 3000^{TM} QQQ mass spectrometer (LC/MS/MS System, equipped with electrospray ion source). A Kinetex C_{18} column (100A pore size, 4.6 mm ID, 2.6 µm particle size, and 10 cm, Phenomenex, Italy) was used for lipid separation. The mobile phase included A: methanol/ water (v/v 7:3) with 10 mM ammonium acetate and B: methanol with 10 mM ammonium acetate. The gradient elution program started from 70% B/30% A, reached 100% B in 45 min, and maintained at 100% B for 20 min. The flow rate was 1 ml/min and 10 µl of sample was injected. The mass spectrometric analysis was carried out in positive ionization mode and MS/MS class-specific scan conditions optimized as follows: NEB (Nebulizer Gas) 9, CUR (Curtain Gas) 10, TEM (Temperature) 300 ^{0}C, IS (IonSpray Voltage) 5 kV, CAD (collision gas) 4, DP (Declustering Potential) 65, FP (Focusing Potential) 250, EP (Entrance Potential) 5, CE (Collision Energy) 40 and CXP (Collision Cell Exit Potential) 18. Unit resolution was set for both Q1 and Q3 and step size was 0.1 amu. Precursor ion scan 184 was used to characterize PC, lyso PC, pPC and SM, indicating the precursor ion form of $[M+H]^+$. Neutral loss scanning of 185, 115, 189, 141 and 277 Da were employed to detect PS with precursor ion $[M+H]^+$, PA with precursor ion $[M+NH_4^+]^+$, PG ($[M+NH_4^+]^+$), PE/ lyso PE/ pPE ($[M+H]^+$) and PI ($[M+NH_4^+]^+$), respectively.

Data processing

Data generated from LC/MS/MS class-specific scanning were processed with Analyst (Version 1.42) by extracting ions from TIC (Total Ion Chromatogram) and peak areas were integrated from EIC (Extracting Ion Chromatogram) after mass tolerance aligning and peak smoothing. Identification of lipid molecular species was resorted to Lipid Mass Spec. Prediction (LIPID MAPS) by surveying Mass, Mass tolerance, Head group and Precursor ion. Intra-class quantification and distribution was assessed by normalizing peak area of each lipid species to the overall area of all lipids belonging to the same lipid class. A data matrix was generated, which comprised of rows representing different samples and columns indicating relative abundance of individual PL species as variables. The data matrix was imported into software SIMCA-P 13.0 (Umetrics, Italy) for multivariate data analysis (MVDA). Pareto-scaling was used to preprocess data and principal component analysis (PCA) was an initial overview of data set about group classification and trends, which here indicated the separation between control and hypoxia-treated HeLa cells. Partial Least Squares Discriminant Analysis (PLS-DA) was used to better discriminate control and treated cells. PLS-DA was also employed to find out PL species as markers which had significant discriminatory power. Unpaired t-test of the candidate marker species was carried out with GraphPad Prism 5. For Unsaturation Index (UI) analysis, the relative abundance of individual PL species was multiplied by their corresponding unsaturation number.

Results and discussion

Cobalt (II) chloride induces hypoxia

Since cellular lipids are highly variable depending on cell cycle, we decided to investigate only the effects of hypoxia on dynamic changes of lipid profile after synchronizing cell growth at the same stage by serum starvation.[16] It has been demonstrated that hypoxia can be induced by $CoCl_2$ and both higher concentration (400 μM) and long term exposure (24h) of $CoCl_2$ induce cell apoptosis.[17] For this reason, we incubated HeLa cells with 200 μM $CoCl_2$ for 3h. Although no apoptosis was observed (data not shown), under this condition, hypoxia was induced. As shown in Fig. 1 hypoxia induction was assessed by monitoring the hypoxia-inducible factor 1-α

(HIF 1-α) which accumulates in the nucleus upon exposure to hypoxic conditions.[18] No morphological changes were observed by microscope analysis after treatment with $CoCl_2$.

NMR analysis of phospholipid classes

The raw lipids extracts obtained from control and hypoxia treated HeLa cells were subjected to extensive 1D (^{1}H and ^{31}P) and 2D (HSQC and HMBC)-NMR measurements carried out at 300 K in deuterated methanol.

The ^{1}H-NMR spectrum contained information which proved to be relevant for arriving at the overall profile of the main cell membrane lipids. In fact, besides the characteristic peaks attributable to the presence of PC (δ_H 3.22 s, δ_C 54.5) and to PE (δ_H 3.16 m, δ_C 41.5), signals due to the presence of plasmenyl PC and/or plasmenyl PE (δ_H 5.96 d and 4.43q, δ_C 146.2 and 108.1, respectively), SM lipids (δ_H 5.71 dt and 5.45d, δ_C 134.9 and 131.0, respectively) were also detected. Moreover, a characteristic triplet at δ_H 3.20 (coupled to δ_C 76.1) was attributed to lipid species belonging to PI class. Worthy of mention, the latter was clearly detectable only in the untreated HeLa samples whilst it was found to be below the detection limit in the hypoxia-treated HeLa samples.

The analysis of these ^{1}H-NMR spectra allowed us i) to clearly detect also cholesterol (Chol) by the presence of the characteristic singlet signals of its angular methyl groups at δ_H 0.72 and δ_H 1.02 (coupled to δ_C 12.2 and δ_C 19.5, respectively) and ii) to establish the [Chol]/[PC+SM lipids] molar ratio by evaluation of the corresponding area of the signal at δ_H 0.72 (x 3) for Chol with respect to the area of the signal at δ_H 3.22 for PC+SM. No statistically significant change of the value of this ratio was found in hypoxia-treated (0.52 ± 0.02) with respect to that of untreated HeLa cell extracts (0.51 ± 0.02).

Although the integration of the ^{1}H-NMR signals allowed to roughly establish also the relative molar ratio of the main PL classes, we used only the results of the corresponding ^{31}P-NMR spectra for the relative quantitative analysis of PL classes in HeLa cell extracts.

The ^{31}P-NMR spectra of untreated (blue spectrum) and $CoCl_2$-treated (red spectrum) HeLa samples are reported in Fig. 2a. The spectral assignment of every resonance to a given PL class was done with reference to the ^{31}P chemical shift scale measured at 300K on 10 mM solutions (CD_3OD as solvent) containing commercially available lipids such as PC, pPC, PE,

pPE, PI, PG, PS and SM. ^{31}P-NMR measurements gave reliable clues to the main PL classes present in the raw HeLa lipid extracts and was used to establish the quantitative changes in PL classes distribution after hypoxia-induced conditions. In particular, the ^{31}P NMR spectra showed the presence of the following classes in order of increasing ^{31}P chemical shifts (δ_P values in ppm, % molar ratio in parenthesis): PC (–0.55, 53%), pPC (–0.49, 6.5%), SM (+0.06, 10%), PE (+0.19, 16.5%), PI and pPE (+0.24, 14%) with the latter two classes, unluckily, not resolved each other in spite of high resolution conditions of our ^{31}P measurements ($W_{1/2} \leq$ 2 Hz). The relative changes in lipid distribution after $CoCl_2$ treatment were obtained by ^{31}P–NMR spectra simulations followed by comparison of the corresponding peak area integrations. As shown in Fig. 2b, a significant decrease was found for the overall amount of PI+pPE, small and opposite trends were found for SM (slight decrease, -10%) and PE (slight increase, +10%) whilst PC and pPC kept almost unchanged. Although a small decrease in the total amount of pPE class was clearly observed in the ^{1}H-NMR spectra, since pPE represented only 2-3% of the overall PL content, the most significant contribution to the decrease of the PI+pPE area (-25%) in the ^{31}P-NMR spectra must be attributed to PI lipid species.

Due to the intrinsically low sensitivity and low dynamic range of NMR measurements, minor PL classes such as PS, PG, lyso PL, ceramides and DAGs were or not detected or not further characterized. Anyhow, NMR spectra of lipids do not contain structural information (i.e. chain length, number of unsaturations, double bonds positions) of the acyl chains present in all PL molecular species. In our study, NMR technique was adopted to estimate inter-class distribution while mass spectrometric analysis was performed to determine intra-class distribution of PL and SL molecular species.

Lipid class-specific (head groups) survey scans through MS/MS measurements

In order to get more comprehensive information about individual PL species, we carried out a detailed mass spectrometric analysis whereby diagnostic fragmentation patterns for all PL classes were established in order to arrive at the complete annotation of lipid species (data not shown). In presence of ammonium ion, the ESI positive ion-mode was found to get clear results for PL identifications; in particular, precursor ion scanning (PIS) of the fragment ion at m/z 184 (phosphocholine head group) was used to identify the protonated molecular ion $[M+H]^+$ of all the PC (including pPC) and the SM lipid species. On the other hand, measurements through the

neutral loss scanning (NLS) of 185, 115, 189, 141 and 277 Da were employed to detect PS, PA, PG, PE and PI, respectively. To sum up, Table 1 showed MS/MS scanning methods with diagnostic fragmentations as well as the corresponding precursor ions for PL identification. These preliminary studies were crucial to establish the class-specific MS/MS methods for PL identification and quantification; a mixture of standard PL from different classes was used for HPLC-ESI MS/MS analysis to validate these methods for sample analysis.

The chromatographic separation and the mass-spectrometric characterization of individual molecular species in the standard PL mixture were optimized by the combination of RP-HPLC (reversed phase liquid chromatography), full scan ESI positive ion-mode assisted by ammonium ions present in the mobile phase and finally by MS/MS precursor ion scanning (PIS) or neutral loss scanning (NLS). As shown in the total ion chromatograms (TIC) in Fig. 3a, the identified PS 18:1/18:1 (by NLS of 185 Da) eluted at 14.04 min while lipids eluted at 20.61 min and 18.31 min were established (PIS of m/z 184) to be PC 18:1/18:1 and SM (d18:1/18:0), respectively. Similarly, PE and PI components were well separated and identified by diagnostic head group survey scan (NLS 141 Da and NLS 277 Da, respectively), which are shown in the TIC in Fig. 3b. Finally, the characterization of PA 18:1/18:1 and PG 18:0/18:0 (by NLS 115 Da and NLS 189 Da, respectively) is shown in Fig. 3c.

Our study confirms that the combination of RPLC and various MS/MS scanning methods is able to target specific PL classes more efficiently than full scan detection.[9,19,20] Moreover, the addition of ammonium ions gives better response factors for each PL class in ESI positive ion-mode by MS/MS with respect to the most used ESI negative ion-mode methodology. Due to ammonium ions in mobile phase, the sodium adducts formation was greatly reduced, leaving the protonated species $[M+H]^+$ for PE and PS and the $[M+NH_4^+]$ adducts for PG, PI and PA as the dominant pseudo-molecular ions, an outcome in keeping with some previous studies.[9,21,22] We also applied this methodology to estimate intra-class PL distribution and to further determine their contributions to the relative changes in lipid composition profile by extra-cellular stimulation.

HeLa cellular phospholipids profiling and hypoxia-induced lipid alterations

The efficiency of total cellular lipid extraction was another key point in order to reliably assess the relative changes upon hypoxia stress. To tackle it, a known amount of PC 12:0/12:0 (DLPC)

was added before solvent extraction (chloroform/methanol 2:1) in order to estimate the recovery both for control and hypoxia-stressed cells. The estimated lipid recovery was about 60% for both control and treated samples.

Our RPLC-ESI (+) MS/MS methodology allowed a direct relative quantitation of the precursor ion mass spectra of all the lipids bearing the phosphocholine groups (PC, SM, lyso PC and plasmenyl PC) contained in HeLa cells after $CoCl_2$ treatment with respect to those from normal HeLa cell cultures; some examples of identified species are presented in Fig. 4a. As a first outcome, no significant changes of these PC species in hypoxia stressed cells were detected (Fig. 4a) as well as for PE and plasmenyl PE (Fig. 4b). The most relevant effect of $CoCl_2$ treatment was instead observed on PI lipids which were found to strongly decrease (almost 3 folds change, Fig. 4c), in good agreement with results from the above reported ^{31}P-NMR experiments. Similar to PC and PE, there were no significant changes of PS lipids (Fig. 4d).

In total, 189 membrane lipid species were characterized, including 42 species of PC, 33 pPC, 13 lyso-PC (LPC), 39 PE, 15 pPE, 14 PI, 10 SM, 10 lyso-PE (LPE), 4 PG and 9 PS. With the class-specific survey scanning, quantitative data were generated from the peak area of detected precursor ions on the assumption that all the species belonging to the same class had almost identical ESI-MS response factors.[9] In particular, the total amount of each class (after normalization by previously added standard DLPC) was evaluated for control and $CoCl_2$ treated HeLa cells. As shown in Fig. 5a, the amount of LPC increased significantly upon hypoxia stimulation (with p value 0.0085) and the same trend was also clear for LPE (Fig. 5b). On the contrary, the overall amount of PI lipids strongly decreased after hypoxia stimulation, which was shown in Fig. 5c. The total amount of PG and DAGs in both control and treated cells was found so low that either a reliable analysis was completely hindered (PG) or their presence (DAG) was uncertain. Concerning PS, a class of membrane lipids expected to play an important role in many cellular signaling, they kept almost unchanged with the exception of PS 36:3 and PS 40:5 after hypoxia treatment (Table 3). Few ceramide-derivatives, namely ceramide (d18:0/C18:0)-1P, ceramide (d18:0/C24:1), ceramide (d18:1/C24:0), 1-galactolsyl-ceramide (d18:1/C24:1) and 1-galactolsyl-ceramide (d18:1/C24:0) were identified but the total amount of all these lipids was less than 1% and remained almost unchanged after the treatment.

Meanwhile, a relative quantitative analysis was performed by normalizing the peak area of each identified lipid to the overall peak area of all lipids belonging to the same class in order

to establish the intra-class distribution of each PL and SL molecular species. The most abundant PC species (% relative abundance in parenthesis) were 34:1 (18.9±1.5), 32:1 (18.7±0.6) and 34:2 (11.1 ± 0.3); the acyl chain length of all the PC species ranged from 28 to 42 whereas the number of double bonds varied from 0 up to 9. Table 2 presented the relative abundances and number of different PL classes in control (C) and hypoxia-treated HeLa cells (T) with a double bond number (N) on the acyl chains higher than 3 or with a double bond number lower than 3. The ratio between polyunsaturated PL species (N ≥3) and PL species with N < 3 varied remarkably in different classes. As shown in Table 2, polyunsaturated PC, pPC and PS species accounted for only 12.4%, 6.1% and 9.4%, respectively whilst the proportion of polyunsaturated species significantly increased in PE (30.9%), pPE (25.6%) and PI (40.1%).

It has been reported that some metabolites which are involved in the biosynthesis and catabolism of phospholipids and other lipids could be affected by the enhanced expression of hypoxia-induced factor (HIF) in hypoxic tumor cell lines, for example, in AML cell lines[23] and prostate cancer cell lines.[24] Generally, hypoxia is able to induce variation in phosphatidylcholine turnover or in myo-inositol level in different cell lines.[23,25,26] For example, it has been reported that under hypoxic conditions, the accumulation of myo-inositol in AML cells might be related to the phosphatidylcholine turnover.[23] Our investigation seems to suggest that the significant decrease of the amount of PI lipids upon hypoxic condition is probably due to the accumulation of cellular myo-inositol, which played a critical role in d*e novo* synthesis of phosphatidylinositol (PI). The changed level of myo-inositol, which has important functions in mammalian cells, has been associated to adjust phospholipid levels.[27] Myo-inositol is also able to participate in up-regulation of glucose metabolism which can affect glycolytic intermediates synthesis.[28] Furthermore, some previous studies have demonstrated that the synthesis of PI from *myo*-inositol was markedly inhibited by hypoxia in the rabbit carotid body.[29] The researchers speculate that during hypoxia several second messenger cascades are activated, which can directly or indirectly influence PI turnover. Another proposed possibility is attributed to the diminution of ATP levels, which is supported by the report that anoxia in isolated hamster heart or permeabilized adrenal chromaffin cells can both cause a decrease in PI biosynthesis paralleled by a decrease in ATP levels.[30,31] Such modulation and variation in cellular PI may indicate an adaptive response in energy homeostasis of hypoxia-stressed HeLa cells.

Multivariate analysis and individual potential marker analysis

As shown in Table 2 there is no clear evidence of difference in the unsaturation distribution within a given class between treated and untreated cells. We wondered if such a difference could become evident by looking at individual phospholipid within a given class under normal or hypoxia conditions. The plots in Fig. 6 illustrate the multivariate data analysis (MVDA) conducted on the 42 phosphatidylcholine species detected in HeLa. Principal component analysis (PCA), an unsupervised multivariate method, was firstly used to analyze the generated MS data. The first two components of PCA model cumulatively described 84% of the total variability. The PCA scores plot (Fig. 6a) showed a clear-cut separation between control and hypoxia-treated HeLa cells in PC2 dimension, thus suggesting that hypoxia treatment induced a significant change in phosphatidylcholine profile. The contribution of each phosphatidylcholine species to the discrimination was further investigated in the corresponding loadings plot (Fig. 6b), which displayed the discrimination pattern. Along the second component to the upper part, the variables represented the more abundant phosphatidylcholine species in hypoxia-treated HeLa cells, whilst in the opposite side are reported the more abundant phosphatidylcholine species in the control cells. On the other hand, mono- or di-unsaturated phosphatidylcholine species are much more representative for the untreated HeLa cells.

Partial least squares discriminant analysis (PLS-DA) model, a supervised multivariate technique, was further applied to enhance class separation and to characterize phosphatidylcholine species responsible for such separation. As illustrated in the PLS-DA scores plot (Fig. 6c), a clearer class separation between control and hypoxia-treated cells could be obtained by the first component. Along the first component of the corresponding loadings plot (Fig. 6d), phosphatidylcholine species further away from the main cluster had stronger influence on class separation[32] and show the most significant changes between control and treated cells. Therefore, the metabolism changes of lipid species associated with hypoxia stimulation could be explained. Further looks at how each phosphatidylcholine specie contributed to the separation could give insights into the importance of each species (variable) and thus variable influence on projection (VIP) plot was displayed (Fig. 6e). This VIP plot summarized the importance of each variable accounting for hypoxia effects. In fact, variables with higher VIP values ($\geq$1) were most influential and accordingly picked out as potential markers (9 candidate phosphatidylcholine

species). In order to confirm that we were dealing with "true lipid markers", univariate analysis (unpaired t-test) was finally carried out.

As shown in the individual marker analysis in Fig. 7, hypoxia-stress induced a remarkable decrease in mono- and di-unsaturated PC species (32:1, 34:2 and 32:2a), whereas polyunsaturated PC species (36:3, 38:5, 36:4a, 38:6a, 38:4c, 38:4a) were increased compared to the corresponding level of control samples. MVDA of PL molecular species from other classes and individual marker analysis were performed in a similar workflow as previously described. The results of MVDA and the univariate confirmation by t-test can show the effects of hypoxia stress on HeLa cells. The identified candidate PL markers and their qualitative changes are presented in Table 3. Moreover, most of LPC and LPE species exhibited pronounced variations and discriminatory power, as reported in Table 4. These analyses showed that hypoxia stress could alter metabolism of PL species from different classes (PC, PE, pPE, pPC, PI, PS, LPC and LPE) and also revealed a general trend induced by hypoxia treatment: PL species with polyunsaturated acyl chains greatly increased whilst mono- and di-unsaturated species reduced. Based on such findings, Unsaturation Index (UI) analysis of each PL class was performed.

Unsaturation Index analysis of each phospholipid class

The intra class unsaturation index (UI) represents the sum of the number of double bonds of each lipid molecular species averaged by their molar fraction within a given class. It was indicated in Fig. 8 that by hypoxia stimulation, UI of LPC, PC, PE and LPE increased (Fig. 8a, b, d and e), while on the contrary, the UI of pPC decreased as compared with the control HeLa cells (Fig. 8c). Results shown in Fig. 8 were in accordance with individual marker analysis presented in Table 3 and 4, which indicated a clear trend of increasing UI for most of the PL molecular species due to hypoxia stress. Such analyses demonstrated that hypoxia had great effect to alter the fatty acid compositions of different classes of PL in HeLa cellular membrane with an overall enhancement of the acyl chain unsaturations.

The membranes lipids are built from fatty acyl chains of various degree of (un)saturation displaying different effects on membrane fluidity and permeability[33] in order to adapt the cell itself to environmental changes. Such adjustment of cellular membrane fluidity might impact several membrane-dependent functions including cell signaling.[34] Previous studies demonstrated

that perturbations of the order-state of membranes were critical for physiological properties of cells such as membrane dynamics as observed in different disease states.[35]

Mechanisms associated with hypoxia-stimulated membrane fluidity and dynamics changes are not clear yet, while such changes might be linked to the enhanced function of fatty-acyl CoA desaturases or the involvement of cellular triglycerides turnover, the unsaturation properties of the latter could also be altered by hypoxia.[36] Another interesting mechanism underlying the alteration of membranes was that the plasma membrane had more abundant sphingolipids, sterols and saturated PL species; instead, the endoplasmic reticulum (ER) contained primarily unsaturated PL species. Such lipids distribution determined that the plasma bilayer membrane was more rigid and impermeable with promoted compartmentalization of specific proteins involved in cellular signaling and cell-cell adhesion. On the other hand, unsaturated PL species would make the ER membrane more fluid and available for the incorporation of newly synthesized proteins.[4] Taken together, the observed increase in membrane PL unsaturation might attribute to the enhanced ER activity in comparison with plasma membrane activity by hypoxia stimulation. In order to confirm this hypothesis, however, a lipidomics analysis on different cell components (plasma, ER, mitochondria, nucleus, and Golgi apparatus) is clearly required but their separation/purification is still a challenging task.

Conclusions

We have developed an RPLC-MS/MS-based methodology for precise identification and characterization of cellular lipids. Cervical cancer derived cells (HeLa cells) were selected as a model to study the effects of hypoxia on tumor lipid profile alterations. Phospholipid profiles of control and hypoxia-stressed cells have been compared by combining NMR and LC-MS data with multivariate and univariate data analysis tools. In particular, our research is the first report of cellular lipidomics study combining NMR with MS technique. Although modern lipidomics approaches mainly rely on the wide arsenal of MS techniques, NMR represents a powerful tool for the qualitative analysis and often it is crucial in the elucidation of their structural details. First of all, the sample preparation for NMR measurements is rather simple and rapid, not implying any derivatization of components. Moreover, NMR analyses carried out on lipids raw extract give an immediate perception of the main lipids therein present. Although the number of compounds detected in a raw lipid extract is limited, the NMR spectra give a good picture of

what really is present, minor compounds might not be seen, but the major trends are clear. In particular, through ^{31}P-NMR it is possible to differentiate the membrane lipids in distinct PL classes and to obtain reliable and reproducible quantitative data such as the molar fractions of all the PL classes. It is worth of mention that in all the (only) MS-based approaches these data are difficult to obtain since PL classes have quite different response factors in ESI source and a direct comparison among all these classes is often hindered by several other factors. Among the latter, neutral membrane lipids (PC, pPC,ePC,SM) are usually detected and quantified in positive ESI ion-mode whilst anionic membrane lipids (PE,PS,PG,PI,CL) require negative ESI ion-mode conditions. The comparison of data obtained in such different conditions is often quite cumbersome and, even worst, eventually unreliable. Of course NMR on lipids shows also some elements of weakness. First, due to its intrinsically low sensitivity, it is necessary to deal with an adequate number of cells, at least a magnitude order higher than used in MS measurements. More importantly, lipids belonging to the same class show almost the same ^{1}H- and/or ^{31}P-NMR spectra no matter of the acyl chain length, number and position of unsaturations. This limitation completely prevents to establish the intra-class chemical diversity. But, the latter information is rather easily achieved by MS measurements, in particular by exploiting the modern LC-MS marriage, making the two techniques highly complementary. In the case discussed here, this joint approach allowed us to characterize up to 189 PL molecular species.

Interestingly, our data showed that hypoxia stimulation significantly reduced the total amount of cellular PI. In contrast, we observed a prominent increase of the amount of LPC as well as LPE in the same samples. Another interesting finding was that hypoxia stress affected cell membrane fluidity and dynamics by increasing the unsaturation of the acyl chains in several lipid classes. Statistical analysis revealed the membranes lipid markers that had discriminatory power. Such analysis might explain the changes of membrane fluidity and dynamics observed in cells in the presence of hypoxia. On the whole, the alterations in lipids amount and the fluidity enhancement in HeLa cellular membrane induced by hypoxia are of vital importance for membrane-dependent functions and the adaptive response of HeLa cells to hypoxia environment. Taken together, our results have proved that lipidomics approach could be explored as an important and integrative tool to investigate effects of stress inducers on lipid distribution and dynamics. Further investigations are required to understand the underlying biochemical

mechanisms whereby lipids distribution can be altered; besides, studies on lipid biosynthesis through the aid of genomics/transcriptomics/proteomics tools will open new perspective for tumor treatment or cancer prevention.[37]

Acknowledgments

We thank Mr. Adriano Sterni (University of Trento) for LC-MS analyses, and technical assistance. We are grateful to dr. Pietro Franceschi (Edmund Mach Foundation, TN) for the helpful discuss and support with the data analysis. The financial supports from Department of Physics and CIBIO (Centre for Integrative Biology) at the Univeristy of Trento are also acknowledged.

Notes and References

1. M. C. Culf, D. A. Barnett, A. S. Culf and I. Chute, *Drug Discov. Today*, 2010, **15**, 610-621.

2. M. R. Wenk, *Nat. Rev. Drug Discov*., 2005, **4**, 594-610.

3. K. Tripathy, *J. Comput. Sci. Syst. Biol.*, 2011, **4**, 93-98.

4. M. B. Khalil, W. M. Hou, H. Zhou, F. Elisma, L. A. Swayne, A. P. Blanchard, Z. M. Yao, S. A. L. Bennett and D. Figeys, *Mass Spectrom. Rev.*, 2010, **29**, 877-929.

5. M. P. Wymann and R. Schneiter, *Nat. Rev. Mol. Cell Biol.*, 2008, **9**, 162-176.

6. M. E. Dumas, E. C. Maibaum, C. Teague, H. Ueshima, B. F. Zhou, J. C. Lindon, J. K. Nicholson, J. Stamler, P. Elliott, Q. Chan and E. Holmes, *Anal. Chem.*, 2006, **78**, 2199-2208.

7. G. F. Pauli, B. U. Jaki and D. C. Lankin, *J. Nat. Prod*., 2005, **68**, 133-149.

8. O. Yanes, R. Tautenhahn, G. J. Patti and G. Siuzdak, *Anal. Chem.*, 2011, **83**, 2152-2161.

9. R. Taguchi, T. Houjou, H. Nakanishi, T. Yamazaki, M. Ishida, M. Imagawa, T. Shimizu, *J. Chromatogr. B*, 2005, **823**, 26-36.

10. X. Li and Y. J. Yuan, *OMICS*, 2011, **15**, 655-664.

11. C. V. Hague, A. D. Postle, G. S. Attard and M. K. Dymond, *Farad. Discuss.*, 2013, **161**, 481-497.

12. C. R. Santos and A. Schulze, *FEBS J.*, 2012, **279**, 2610-2623.

13. A. J. Giaccia, M. C. Simon and R. Johnson, *Genes Dev.*, 2004, **18**, 2183-2194.

14. A. M. Weljie and F. R. Jirik, *Int. J. Biochem. Cell Biol.*, 2011, **43**, 981-989.

15. E. G. Bligh and W. J. Dyer, *Biochem. Cell Biol.*, 1959, **37**, 911-917.

16. C. V. Hague, PhD thesis, Faculty of Engineering, Science and Mathematics, *University of Southampton*, 2009, 271 pp.

17. S. J. Yang, J. Pyen, I. Lee, H. Lee, Y. Kim and T. Kim, *J. Biochem. Mol. Biol.*, 2004, **37**, 480-486.

18. G. L. Semenza, *Curr. Opin. Cell Biol.*, 2001, **13**, 167-171.

19. X. Han, J. Yang, H. Cheng, H. Ye and R.W. Gross, *Anal. Biochem.*, 2004, **330**, 317-331.

20. K. Ekroos, I. V. Chernushevich, K. Simons and A. Shevchenko, *Anal. Chem.*, 2002, **74**, 941-949.

21. M. Koivusalo, P. Haimi, L. Heikinheimo, R. Kostiainen and P. Somerharju, *J. Lipid Res.*, 2001, **42**, 663-672.

22. J. V. Busik, G. E. Reid and T. A. Lydic, *Methods Mol. Biol.*, 2009, **579**, 33-70.

23. A. Lodi, S. Tiziani, F. L. Khanim, M. T. Drayson, U. L. Gűnther, C. M. Bunce and M. R. Viant, *ACS Chem. Biol.*, 2011, **6**, 169-175.

24. K. Glunde, T. Shah, P. T. Winnard, V. Raman, T. Takagi, F. Vesuna, D. Artemov and Z. M. Bhujwalla, *Cancer Res.*, 2008, **68**, 172-180.

25. E. Ackerstaff, D. Artemov, R. J. Gillies and Z. M. Bhujwalla, *Neoplasia*, 2007, **9**, 1138-1151.

26. F. Podo, *NMR Biomed.*, 1999, **12**, 413-439.

27. A. Ferretti, S. D'Ascenzo, A. Knijn, E. Iorio, V. Dolo, A. Pavan and F. Podo, *Br. J. Cancer*, 2002, **86**, 1180-1187.

28. R. Mendelsohn, P. Cheung, L. Berger, E. Partridge, K. Lau, A. Datti, J. Pawling and J. W. Dennis, *Cancer Res.*, 2007, **67**, 9771-9780.

29. R. Rigual, M. T. G. Cachero, A. Rocher and C. González, *Pflügers Arch., Eur. J. Physiol.*, 1999, **437**, 839-845.

30. J. T. Wong, R. Y. K. Man and P. C. Choy, *Lipids*, 1996, **31**, 1059-1067.

31. D. A. Eberhard, C. L. Cooper, M. G. Low and R. W. Holz, *Biochem. J.*, 1990, **268**, 15-25.

32. H. Zhang, J. R. Wang, L. F. Yau, H. M. Ho, C. L. Chan, P. Hu, L. Liu and Z. H. Jiang, *Mol. BioSyst.*, 2012, **8**, 3208-3215.

33. E. Busse, G. Zimmer, O. Bartsch and B. Kornhuber, *Oncology*, 1993, **50**, 241-244.

34. E. J. Helmreich, *Biophys. Chem.*, 2003, **100,** (1-3), 519-534.

35. J. M. Ntambi, *Prog. Lipid Res.*, 1995, **34**, 139-150.

36. M. Ståhlman, C. S. Ejsing, K. Tarasov, J. Perman, J. Borén and K. Ekroos, *J. Chromatogr. B*, 2009, **877**, 2664-2672.

37. T. Mashima, H. Seimiya and T. Tsuruo, *Br. J. Cancer*, 2009, **100**, 1369-1372.

Legends to Figures

Fig. 1 $CoCl_2$-induced hypoxia in mammalian cells. HIF 1-α is a cytoplasmic protein. HeLa cells lines were treated with 200 μM cobalt chloride for 3h and then processed for immunostaining analysis. Fluorescent images were taken from representative cells. (a) Immunostaining for HIF 1-α (red) and ACTIN (green) shows the cytoplasmatic localization of HIF 1-α in normoxia conditions. (b) Under hypoxia induction, HIF 1-α shuttles from the cytoplasm and localizes within the nucleus. (63X magnification).

Fig. 2 NMR analysis of PL composition in control and hypoxia-stressed HeLa extracts. (a) Overlay of the high resolution ^{31}P-NMR spectra of untreated (blue) and hypoxia-stressed (red) HeLa extracts (b) Relative % changes of selected PL classes.

Fig. 3 RPLC MS/MS determination of standard lipid mixtures (DOPC, DOPS, DOPA, DSPG, SM (Brain, Porcine), L-α-PE (Egg, Chicken), L-α-PI (Soy)) in ESI positive mode. (a) Detection of DOPS by NLS at 185 Da and DOPC, SM (d18:1/18:0) by PIS of m/z 184; (b) Identification of PE 34:1 by NLS of 141 Da and PI 34:2 by NLS of 277 Da; (c) Detection of DOPA by NLS of 115 Da and DSPG by NLS of 189 Da.

Fig. 4 Ion chromatograms obtained by LC-MS analysis of control HeLa cellular lipids (designated as "C", left) and $CoCl_2$-treated HeLa cellular lipids (designated as "T", right) for (a) top: PC, SM, LPC and pPC, as detected through PIS of m/z 184; bottom: lipid species detected within the time retention windows 13.01–13.12 min (C) and 13.52–13.62 min (T); (b) PE, pPE and LPE, as detected through NLS of 141 Da; (c) PI as detected through NLS of 277 Da; d) PS as detected through NLS of 185 Da. Note that the intensities of PI signals in treated are almost 3 times lower than in untreated HeLa cells.

Fig. 5 Amount **o**f overall PL classes (values expressed in term of areas obtained from MS/MS experiments) of control and hypoxia-stressed HeLa cells. Upon hypoxia treatment (a) LPC increases, (b) LPE increases and (c) PI decreases. The superscript (*) shows significant differences of treated (T) with respect to control (C) at $p < 0.05$ (n=4).

Fig. 6 Multivariate data analysis of 42 species of HeLa cellular phosphatidylcholine (PC). (a) PCA scores plot, and (b) Loadings plot of the control and hypoxia-treated HeLa cells (designated as "C" and "T" respectively, n=4) (c) PLS-DA scores plot and (d) Loadings plot (e) VIP plot from PLS-DA.

Fig. 7 Univariate analysis of potential PC markers obtained from PLS-DA. Mono- or di-unsaturated PC (32:1, 34:2, 32:2a) decreased whilst poly-unsaturated PC species (36:3, 38:5, 36:4a, 38:6a, 38:4c, 38:4a) increased upon hypoxia stress. The superscript (*) shows significant differences of treated (T) with respect to control (C) at $p < 0.05$ (n=4).

Fig. 8 Unsaturation Index (UI) analysis for each PL class. By hypoxia treatment UI of (a) LPC, (b) PC, (d) PE and (e) LPE increased whilst (c) pPC decreased. The superscript (*) shows significant differences of treated (T) with respect to control (C) at $p < 0.05$ (n=4).

Table 1 Characteristic fragmentation patterns of each PL class

Phospholipid Class	Precursor Ion	MS/MS Type	Characteristic Fragment
Phosphatidylcholine (PC)	$[M+H]^+$	Precursor ion scan (PIS) 184	Phosphocholine
Sphingomyelin (SM)	$[M+H]^+$	PIS 184	Phosphocholine
Phosphatidylethanolamine (PE)	$[M+H]^+$	Neutral loss scan (NLS) 141	Phosphoethanolamine
Phosphatidylserine (PS)	$[M+H]^+$	NLS 185	Phosphoserine
Phosphatidylinositol (PI)	$[M+NH_4^+]^+$	NLS 277	Phosphoinositol $+NH_3$
Phosphatidylglycerol (PG)	$[M+NH_4^+]^+$	NLS 189	Phosphoglycerol $+NH_3$
Phosphatidic acid (PA)	$[M+NH_4^+]^+$	NLS 115	Phosphoric acid $+NH_3$

Table 2 Relative abundances and number of species of different PL classes in control (C) and hypoxia-treated HeLa cells (T) with a double bond number (N) on the acyl chains higher than 3 or with a double bond number lower than 3.

Double Bonds	PC		pPC		PE		pPE		PI		PS	
	Relative abundance (%)	Nr. of species	Relative abundance (%)	Nr. of species	Relative abundance (%)	Nr. of species	Relative abundance (%)	Nr. of species	Relative abundance (%)	Nr. of species	Relative abundance (%)	Nr. of species
N ≥ 3 (C)	12.4 ± 0.7	***27***	6.1 ± 0.6	***6***	30.9 ± 1.1	***26***	25.6 ± 1.6	***6***	40.1 ± 3.0	***8***	9.4 ± 1.1	***3***
N < 3 (C)	87.6 ± 0.7	***15***	93.9 ± 0.6	***27***	69.1 ± 1.1	***13***	74.4 ± 1.6	***9***	59.9 ± 3.0	***6***	90.6 ± 1.1	***6***
N ≥ 3 (T)	16.0 ± 1.4	*27*	5.4 ± 0.3	*6*	32.6 ± 1.4	*26*	25.2 ± 1.4	*6*	42.1 ± 3.4	*8*	9.3 ± 0.5	*3*
N < 3 (T)	84.0 ± 1.4	*15*	94.6 ± 0.3	*27*	67.4 ± 1.4	*13*	74.8 ± 1.4	*9*	57.9 ± 3.4	*6*	90.7 ± 0.5	*6*

Table 3 Identified potential PL markers and their corresponding qualitative changes in hypoxia-treated (T) or control HeLa cells (C).

Lipid Class	Identity of PL molecular species	Higher abundance in Control (C) or Treated (T)
PE	PE 34:2	C
Plasmenyl PE	pPE 34:1	T
Plasmenyl PE	pPE 36:5	C
Plasmenyl PE	pPE 38:6	T
Plasmenyl PC	pPC 36:2	T
Plasmenyl PC	pPC 36:1	T
Plasmenyl PC	pPC 36:3	C
Plasmenyl PC	pPC 34:2	T
Plasmenyl PC	pPC 36:5	C
Plasmenyl PC	pPC 38:6	C
PI	PI 32:1	C
PI	PI 38:4	T
PI	PI 38:3	T
PS	PS 36:3	T
PS	PS 40:5	C

Table 4 Potential LPC, LPE markers and their corresponding distributions in hypoxia-treated or control HeLa cells

Lipid Class	Identity of PL molecular species	Higher abundance in Control (C) or Treated (T)
LPC	LPC 20:1, LPC 22:5, LPC 14:0, LPC 22:6, LPC 22:4, LPC 16:1, LPC 20:5, LPC 18:2, LPC 20:3	T
LPE	LPE 20:4, LPE 22:5, LPE 22:4, LPE 20:3, LPE 24:4,	T
LPE	LPE 18:0, LPE 18:1	C

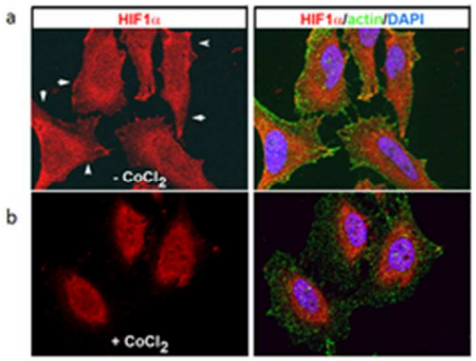

19x15mm (300 x 300 DPI)

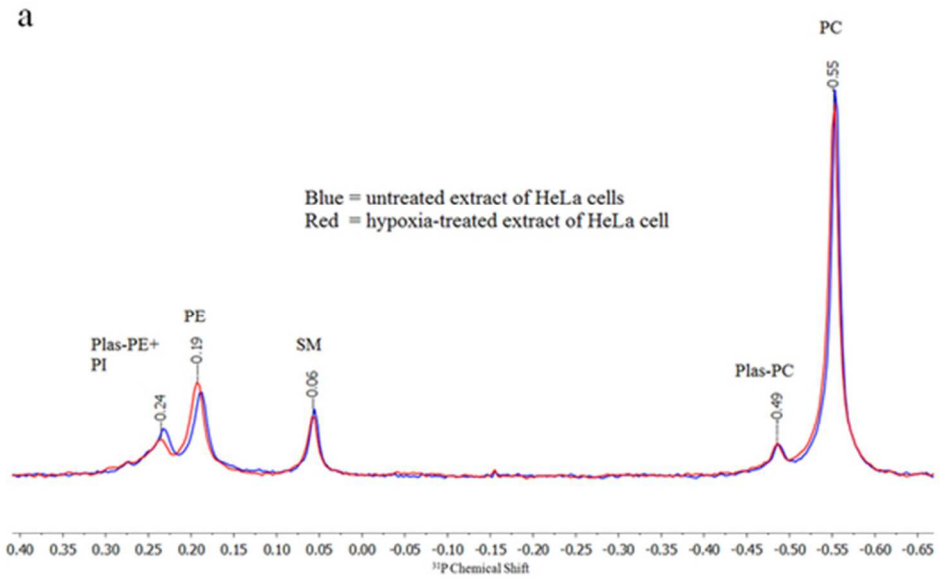

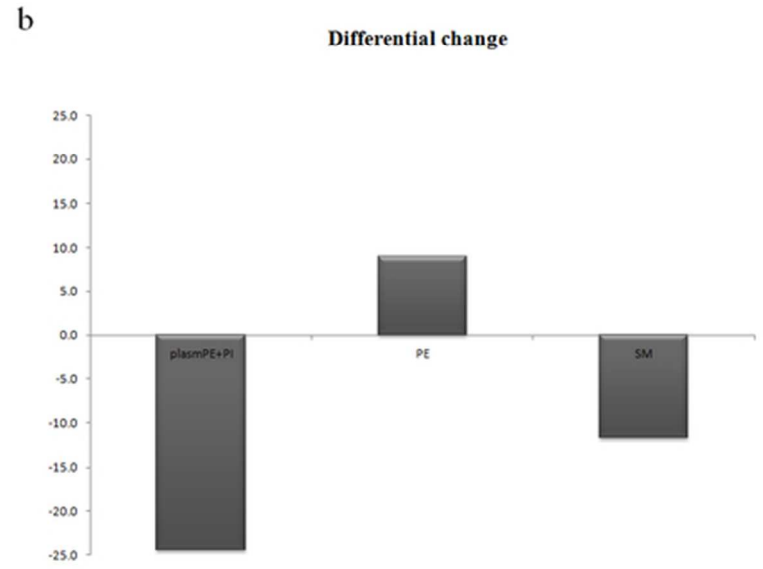

48x61mm (300 x 300 DPI)

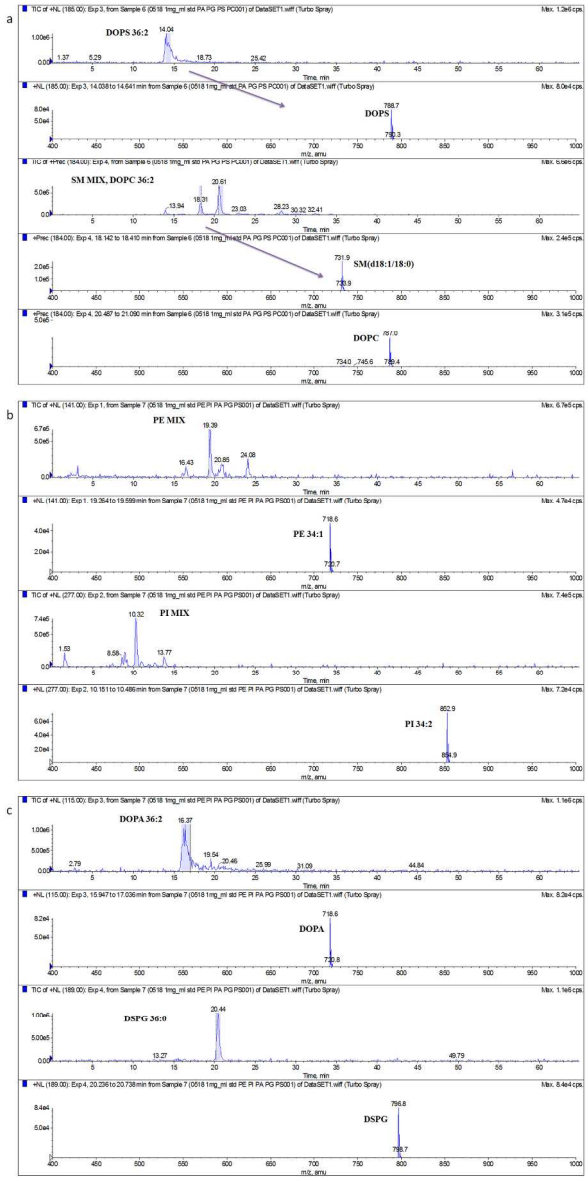

134x262mm (300 x 300 DPI)

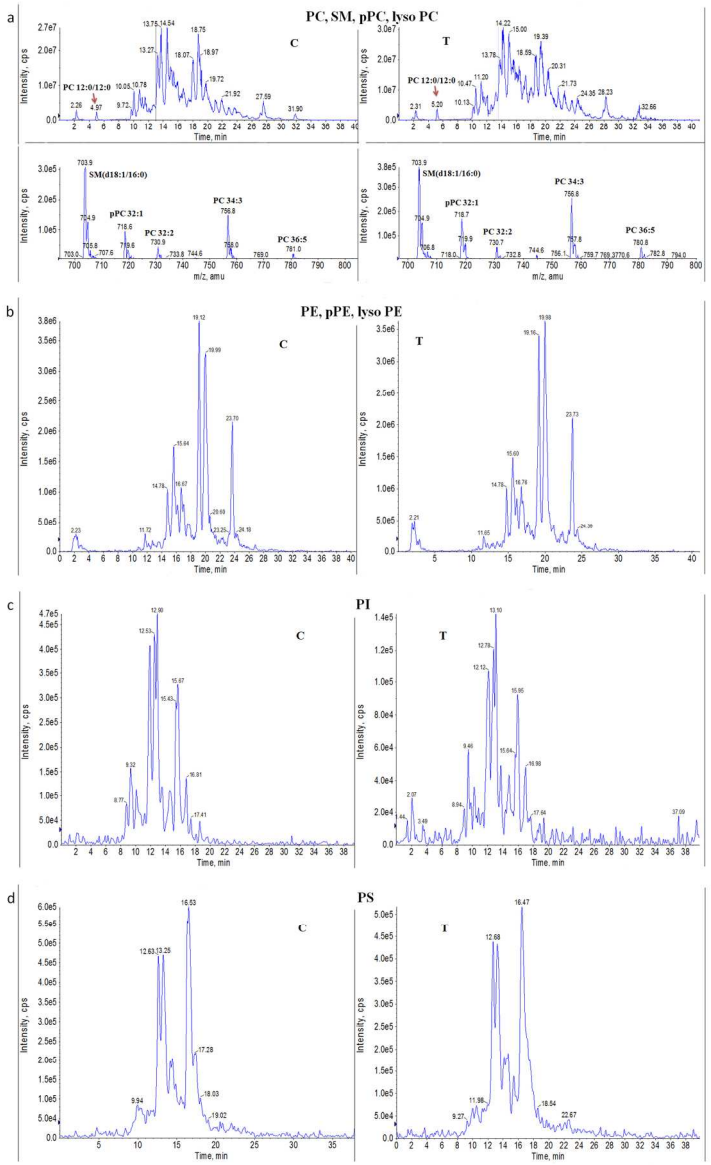

126x205mm (300 x 300 DPI)

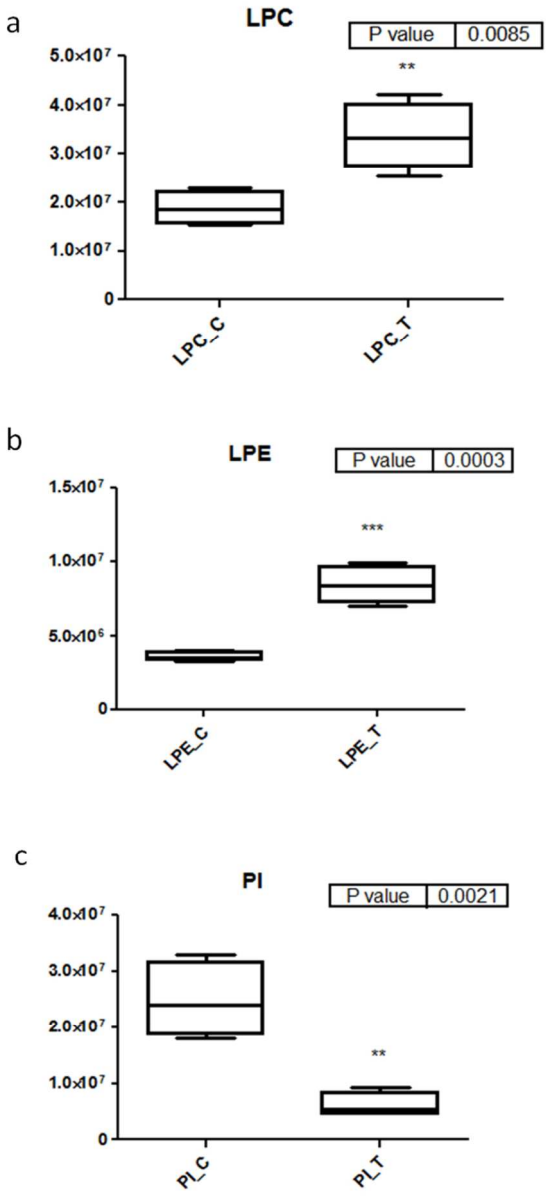

61x130mm (300 x 300 DPI)

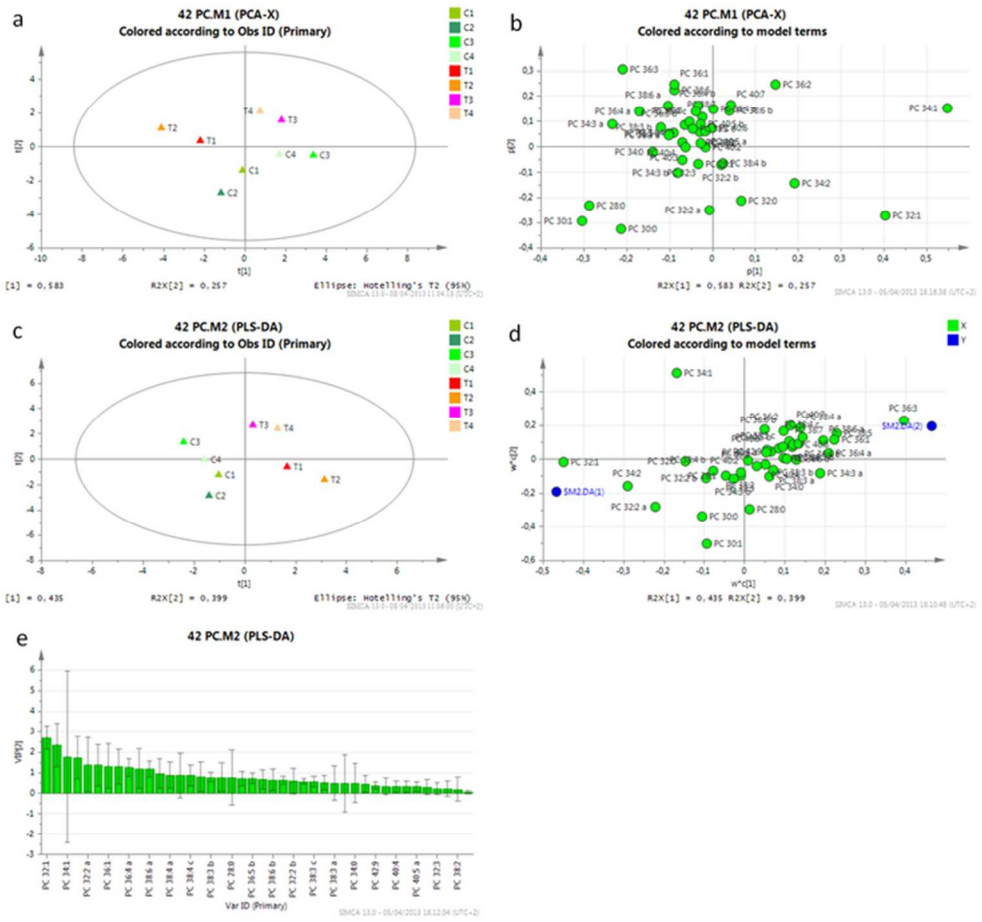

63x59mm (300 x 300 DPI)

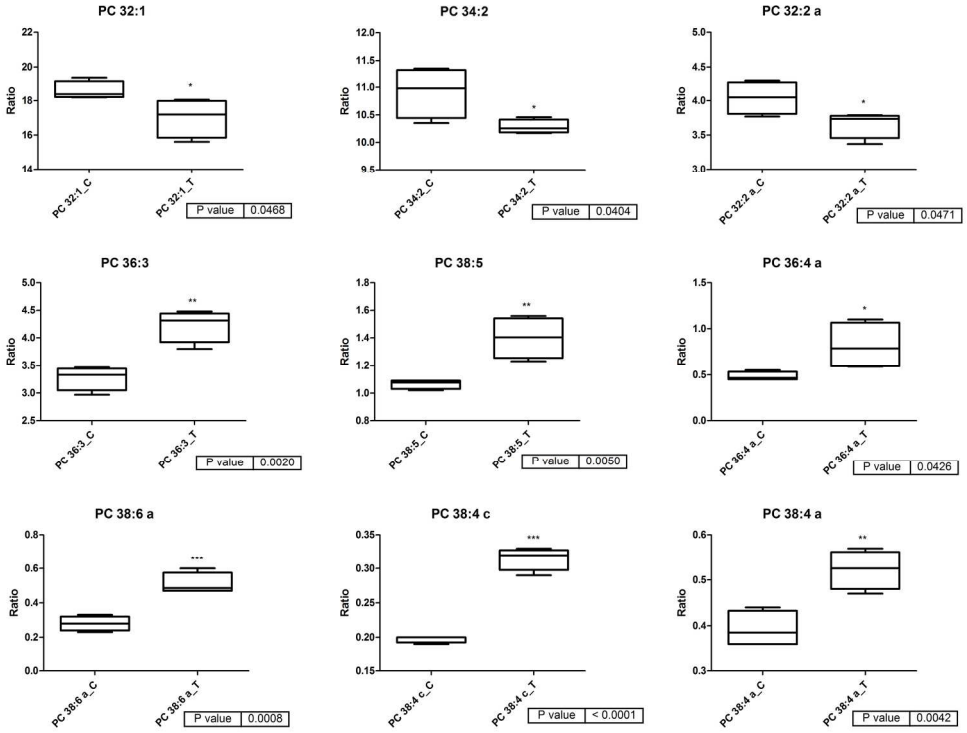

197x151mm (300 x 300 DPI)

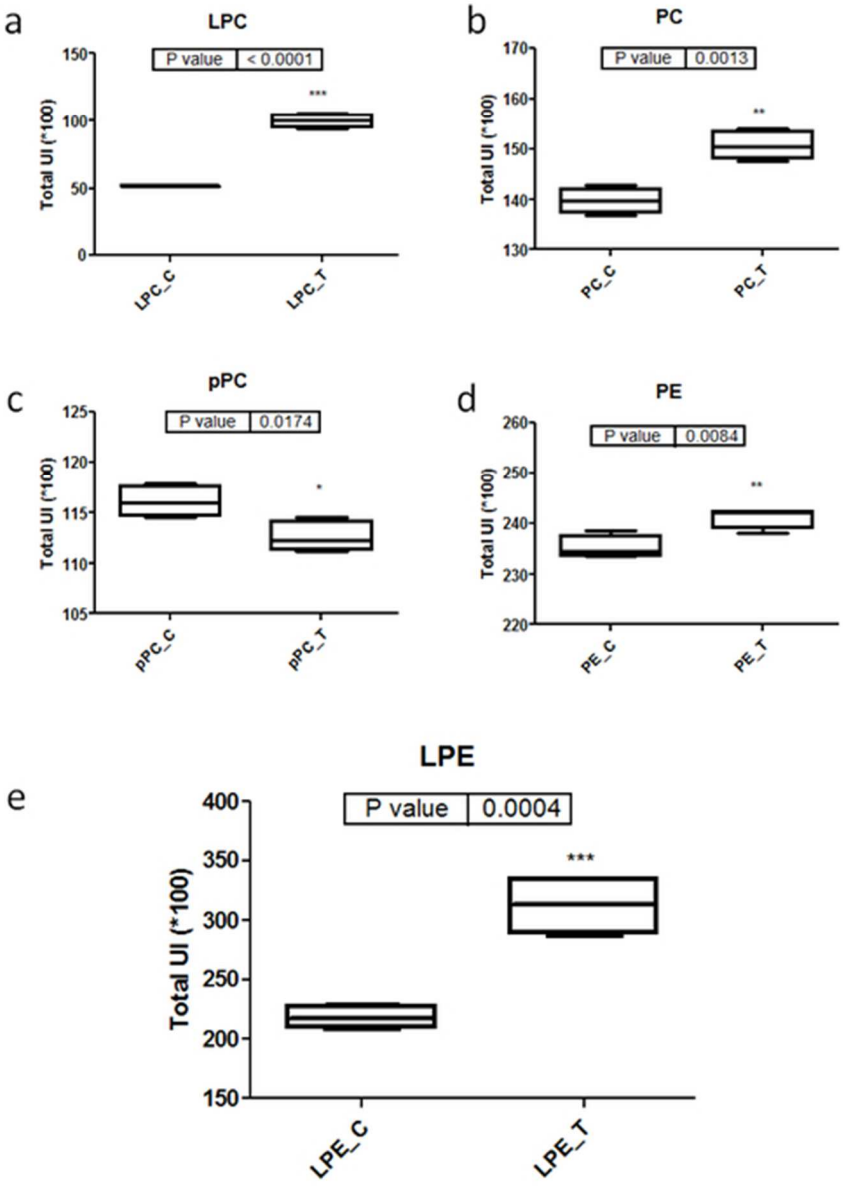

42x58mm (300 x 300 DPI)